

## Article

# Organic Acids from Glucose—Heterogeneous Catalysis with the Participation of Natural Zeolite

Natalia Sobuś<sup>1,\*</sup> , Igor Łabaj<sup>1</sup> and Magdalena Król<sup>2,\*</sup> 

<sup>1</sup> Faculty of Chemical Engineering and Technology, Cracow University of Technology, Warszawska 24, 31-155 Krakow, Poland

<sup>2</sup> Faculty of Materials Science and Ceramic, AGH University of Science and Technology, 30 Mickiewicza Av., 30-059 Krakow, Poland

\* Correspondence: natalia.sobus@pk.edu.pl (N.S.); mkrol@agh.edu.pl (M.K.)

**Abstract:** In this paper, we present the results of a one-pot process for converting, utilizing a modified clinoptilolite catalyst. Iron, cobalt, and copper were introduced into the zeolite structure as active centers. The modified clinoptilolite catalyst was characterized in terms of phase composition, structure, and microstructure (using XRD, BET, FT-IR, and DRS UV-VIS), as well as the speciation of introduced metals. The catalytic process was conducted at a temperature of 250 °C for 1–5 h. Depending on the catalyst used and the specific process conditions, the reaction mixture exhibited the formation of various organic acids, including lactic acid (100% yield after 1 h using CLI), levulinic acid (40.3% yield after 5 h using Fe-H-CLI), formic acid (15.8% yield after 3 h using Fe-H-CLI), and acrylic acid (11.9% yield after 5 h using Fe-CLI).

**Keywords:** zeolite; clinoptilolite; heterogeneous catalyst; biomass conversion; glucose; organic acids; lactic acid



**Citation:** Sobuś, N.; Łabaj, I.; Król, M. Organic Acids from Glucose—Heterogeneous Catalysis with the Participation of Natural Zeolite. *Catalysts* **2023**, *13*, 1202. <https://doi.org/10.3390/catal13081202>

Academic Editors: Mário Manuel Quialheiro Simões and Leonarda Liotta

Received: 30 June 2023

Revised: 1 August 2023

Accepted: 8 August 2023

Published: 11 August 2023



**Copyright:** © 2023 by the authors. Licensee MDPI, Basel, Switzerland. This article is an open access article distributed under the terms and conditions of the Creative Commons Attribution (CC BY) license (<https://creativecommons.org/licenses/by/4.0/>).

## 1. Introduction

The transformation of glucose into organic acids has garnered considerable attention in recent years due to its relevance in sustainable chemistry and the potential to produce valuable chemical compounds from renewable resources. Organic acids play a pivotal role in various industries, including pharmaceuticals, food, and biofuels, and their production through eco-friendly routes has become an area of intense research. Glucose, as a prominent and abundant carbohydrate derived from biomass, serves as an ideal precursor for the synthesis of organic acids. The transformation of glucose into organic acids can occur via various reaction pathways (Figure 1). Irrespective of the carboxylic acid obtained during biomass valorization, the initial step involves the isomerization reaction of C6 sugars glucose (GLU) to fructose (FRU) facilitated by Lewis acid centers [1,2]. In the case of obtaining levulinic acid (LA) or a mixture of LA and formic acid (FA), the intermediate product is 5-HMF, which forms from the dehydration of the glucose isomer using Brønsted acid centers. Subsequently, hydration leads to the formation of LA and FA [3,4]. An alternative pathway for GLU-FRU isomerization involves the production of intermediate product(s) such as dihydroxyacetone (DHA) and/or glyceraldehyde (Gly-AD) [5]. DHA and/or Gly-AD formation occurs through a re-aldol reaction from fructose [6]. The presence of DHA and/or Gly-AD results in the generation of oxalic acid during their oxidation reaction [7,8]. Furthermore, it is possible to obtain lactic acid (LAC) from the conversion of the DHA/Gly-AD mixture [9–11]. This conversion proceeds via the dehydration reaction to the intermediate product pyruvaldehyde (Py-AD), followed by hydration to produce LAC [12]. LAC can also be transformed into acetic acid (AC) via a two-stage process involving decarbonylation/decarboxylation and oxidation reactions [13,14] or into acrylic acid (AA) via the dehydration of LAC [15].

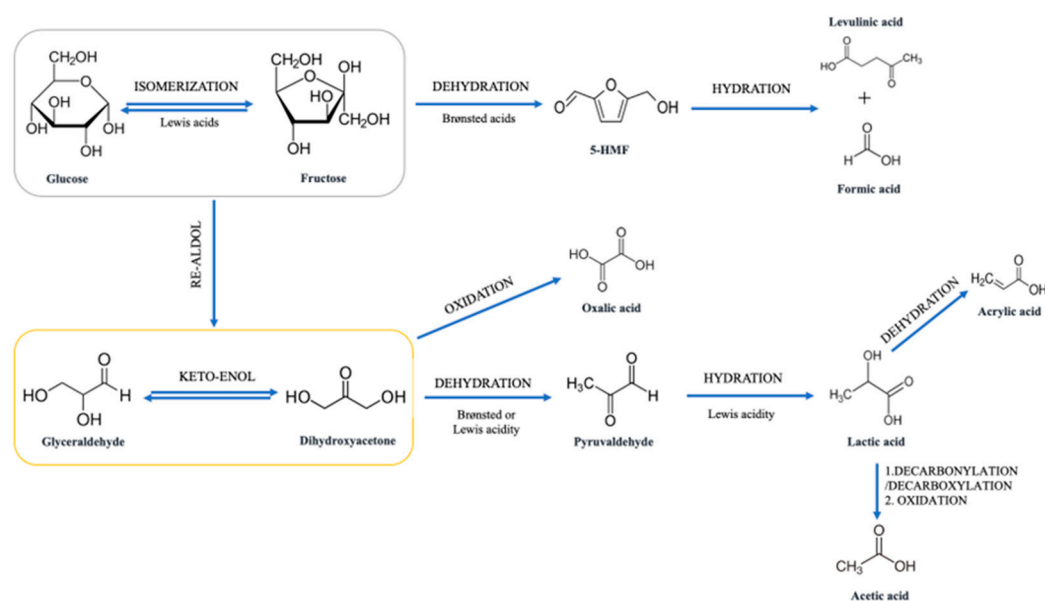


**Figure 1.** Potential pathways for the transformation of glucose into organic compounds [16–18].

Proposed conditions for glucose conversion processes involving catalysts have been suggested [19–21]. Ramesh et al.'s [19] study explores the application of a composite material based on Ti-Al<sub>2</sub>O<sub>3</sub> with an Al/Ti ratio of 10, which was synthesized using the sol-gel method. Precursors such as sulfuric acid, thiourea, and dibenzyl polysulfide (DBPS) were employed. Under these conditions, glucose conversion catalysis yielded 5-HMF with a 97% conversion rate and a 65% yield after a 4 h reaction at 170 °C. Another potential catalyst material, proposed by Li et al. [20], is a composite comprising a 5-sulfoisophthalic acid ligand with tin (SnPCP) and coated with polydopamine MnO<sub>2</sub> (MnO<sub>2</sub>-PDA). This composite demonstrated a glucose to 5-HMF conversion rate of 55.8% in DMSO and 41.2% in water/THF. On the other hand, Atanda et al. [21] conducted the process using a phosphate catalyst based on TiO<sub>2</sub> in a two-phase water-butanol system. After a 3 h reaction at 175 °C, the catalyst achieved an 81% HMF yield and 97% raw material conversion.

Another potential chemical that can be obtained during biomass valorization in the presence of GLU is levulinic acid (LA). Kumar's work [22] focused on developing conditions for the catalytic conversion of GLU to LA. Ionic liquids based on 2-phenyl-2-imidazoline and employed various anions (NO<sub>3</sub><sup>-</sup>, H<sub>2</sub>PO<sub>4</sub><sup>-</sup>, and Cl<sup>-</sup>) with Brønsted acid active centers were utilized. The conversion process achieved a 98% LA maximum yield during a 3 h reaction at 180 °C. Homogeneous catalysis employing sulfuric acid at different concentrations (0.05–1 M) and GLU as the raw material (0.1–1 M) is another possibility [23]. Furthermore, phosphate catalysts with metal(IV) elements, such as zirconium and tin phosphates, with varying phosphorus-to-metal(IV) ratios, were employed [24].

Another compound that can be generated via the catalytic conversion of glucose (GLU) is lactic acid (LAC). Shen's research [25] explores the potential utilization of acid-base bifunctional Sn-Beta-NH<sub>2</sub> catalysts by grafting aminopropyl groups onto the surface silanol groups of Sn-Beta zeolite. The resulting catalyst was then used in glucose conversion. The process was carried out at 190 °C for 2 h, during which the identification of the products took place using HPLC with a UV detector. The conversion of the raw material and the yield of the products were determined. Sugar conversion was defined as the number of moles of feedstock reacted divided by the number of moles used in the process. In turn, the yield of the product was determined based on the carbon content. Based on the calculations, it was determined that the raw material was fully reacted to obtain lactic acid (LAC) with a yield of 56%. Additionally, the yield of the intermediate product—5-methylhydrofurfural (5-MHF)—was also determined to be 7%.

Another example of lactic acid production involves the process of cellulose conversion using a bifunctional Al(III)-Sn(II) catalyst with a molar ratio of 1:1 [26]. The process was carried out in a stainless steel autoclave, where powdered cellulose, a catalyst at various concentrations, and deionized water were introduced. N<sub>2</sub> was also introduced into the reactor at a pressure of 3 MPa, and the reactor was placed in an oil bath heated to 190 °C. The reactor contents were stirred, and after 2 h, the reactor was removed from the bath and cooled to room temperature. The resulting reaction products were then analyzed by HPLC with an RI detector. Feed conversion was defined as the difference in moles of feedstock before and after the process. In turn, the yield of the products was determined as the percentage of moles of carbon in the products compared to the moles of carbon in the raw material. Based on the results, it was determined that the conversion of the raw material and the yield of the product—lactic acid (LAC)—increased depending on the increase in the molar concentration of the catalyst. The highest yield, approximately 80%, was obtained using a catalyst with a concentration of 5.1 mmol/dm<sup>3</sup>, with the conversion of the raw material achieved at the same level. However, it was noted that a further increase in the catalyst concentration to 12 mmol/dm<sup>3</sup> did not lead to a higher yield of lactic acid, but only resulted in a slight increase in cellulose conversion to the range of 81–85%.

Lactic acid was also produced during the conversion of glucose using the Sn-BEA catalyst [27]. The process was conducted in a stainless-steel reactor, into which 0.15 g of raw material, 0.2 g of catalyst, and 7.35 ml of water were introduced. Subsequently, the autoclave was sealed and heated at 200 °C in an oil bath for 30 min at a helium pressure of 4.0 MPa. The contents of the autoclave were stirred at 600 rpm. Afterward, the reactor was cooled to room temperature. The products formed after the process were analyzed by HPLC-RID and confirmed by GC-MS. The conversion of the raw material was determined based on the results obtained from the HPLC analysis, calculated as the difference between moles of carbon in glucose and the number of moles of carbon determined by the HPLC method, divided by the number of moles of carbon in glucose, and then multiplied by 100%. On the other hand, the yield of the products was defined as the amount of moles of carbon determined by HPLC divided by the amount of moles of carbon in glucose, multiplied by 100%. Based on the obtained results, it was determined that the yield of lactic acid under the proposed conditions was 67.1%, with the conversion of the raw material exceeding 98%.

Based on the related literature review, it was found that further research on glucose conversion processes into various chemical compounds is necessary. This article describes the conditions for catalytic glucose conversion using a modified zeolite of natural origin, specifically clinoptilolite. The significant advantages of employing this type of catalytic material include non-toxicity, the ability to create active centers, as well as its availability and affordability. Furthermore, it is essential that the transformation process of all raw materials occurs without the presence of toxic solvents whenever possible. To address this concern, this article proposes optimal conditions for glucose conversion using natural zeolite without the need for any solvents. The clinoptilolite was subjected to ammonium exchange to enhance its specific surface area and improve its ion exchange properties. This modification aimed to create a potentially suitable matrix for the following active centers: iron, copper, and cobalt. Additionally, clinoptilolite was utilized as the catalyst without any further modifications. The glucose conversion process took place at a temperature of 250 °C for durations of 1, 3, and 5 h. The catalytic tests, conducted within these time intervals, aimed to assess the catalytic activity of the zeolite materials and identify the products formed during the process at specific times. In addition to the proposed conditions for the glucose conversion process, it was investigated whether modifying the catalyst matrix via the hierarchization of clinoptilolite and the use of different metals (Cu, Co) had an impact on the given process. This article also presents the physicochemical characteristics of the zeolite catalysts and provides information on the selectivity and yields of the obtained products during the catalytic tests, where glucose (GLU) was used as the raw material.

## 2. Results

Figure 2 displays the X-ray diffraction (XRD) patterns illustrating the clinoptilolite before and after modifications. The zeolite primarily comprises clinoptilolite, and additionally, there are minor quantities of other phases present, including quartz, cristobalite, illite, feldspar, and kaolinite. Compared to the initial CLI sample, after performing ion exchange and calcination on the sample (H-CLI), it is evident that the zeolite phase and feldspar content have increased. The process of washing the zeolite led to the elimination of finer mineral fractions, while calcination helped remove impurities. Based on the obtained data, there is no indication of an increase in amorphism in the hydrogen form of the zeolite. The obtained results indicate that the proposed modification procedure does not destroy the zeolite structure.

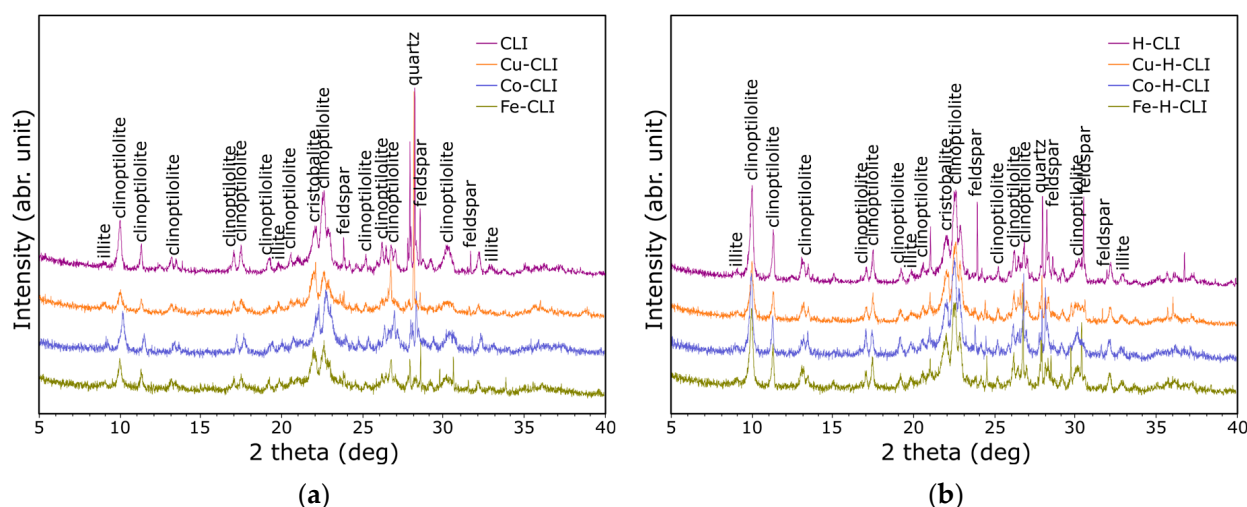


**Figure 2.** XRD patterns of zeolite catalysts after ion exchange on the initial form (a) and on the hydrogen form (b) of clinoptilolite.

Based on the XRD patterns obtained for clinoptilolite for which ion exchange was carried out on the initial form (CLI; Figure 2a), it is evident that the intensity of the bands remains unchanged. This observation serves as evidence that the crystal structure is still preserved and that there is no significant increase in the amount of amorphous phase induced by ion exchange. XRD patterns for samples prepared with the used hydrogen form of clinoptilolite are collected in Figure 2b. In this case, it can be noticed that ultrasound treatment led to a reduction in the peak intensity compared to the starting sample (H-CLI). The reduction in peak intensities for these samples proves partial structure degradation. However, the preserved crystalline structure of clinoptilolite can still be observed.

Figure 3 presents a comparison of the FT-IR spectra of the following different clinoptilolite samples: clinoptilolite without modification (CLI; Figure 3a) and after ammonium exchange and calcination (H-CLI; Figure 3b). Although the differences in the spectra are minor, they provide significant information regarding the structural changes induced by zeolite modification. The most prominent bands at about  $1080\text{ cm}^{-1}$  are attributed to vibrations of internal Si–O(Si) and Si–O(Al) bonds, which exist in tetrahedra [28]. This band actually consists of several component bands. Its peak position shifts towards higher wavenumbers from the parent zeolite spectrum (CLI) to the spectrum of its hydrogen form (H-CLI). Additionally, a disappearance of the shoulder at approximately  $1040\text{ cm}^{-1}$  is observed following the same trend. This shift may, on the one hand, be caused by the removal of clay minerals during several treatments with aqueous solutions. On the other hand, it may indicate a strong binding of the metal cation to the structure of the zeolite [29]. There is also a clear change in the integral intensity of the band at about  $915\text{ cm}^{-1}$  attributed to the silanol groups (Si–OH). This band disappears after the ion exchange process. The observed change proves the possible attachment of metal cations to the silanol group. Thus,

it proves the incorporation of metal cations into the structure of the zeolite and the possible formation of active centers.

The remaining bands in the spectrum show minimal changes in both position and intensity. The band observed at  $1642\text{ cm}^{-1}$  can be attributed to the bending vibrations of the H–O–H group, which is characteristic of the presence of zeolite water in the analyzed samples [30,31]. The doublet of bands around  $798\text{ cm}^{-1}$  indicates the presence of quartz in the samples. The remaining bands correspond to vibrations occurring within the aluminosilicate structure.

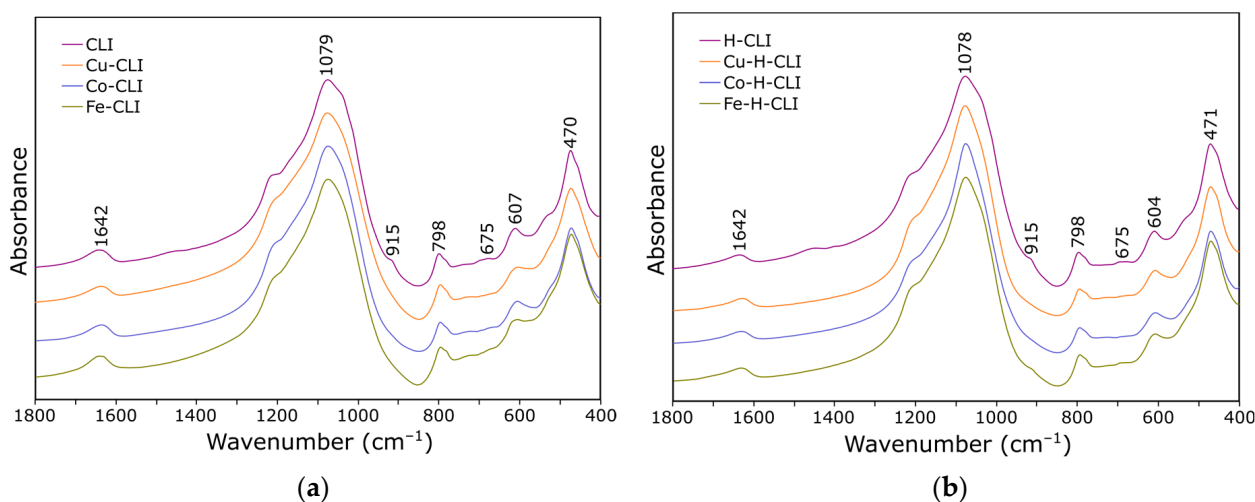


**Figure 3.** FT-IR spectra of zeolite catalysts after ion exchange on the initial form (a) and on the hydrogen form (b) of clinoptilolite.

Figure 4 presents the nitrogen adsorption/desorption isotherms for the clinoptilolite-based catalyst. From the results, it is observed that all the samples, including the reference material and those with different metal ions, exhibit a mesoporous nature. The isotherms can be classified as IUPAC type IV [32]. The materials have a mesoporous structure.

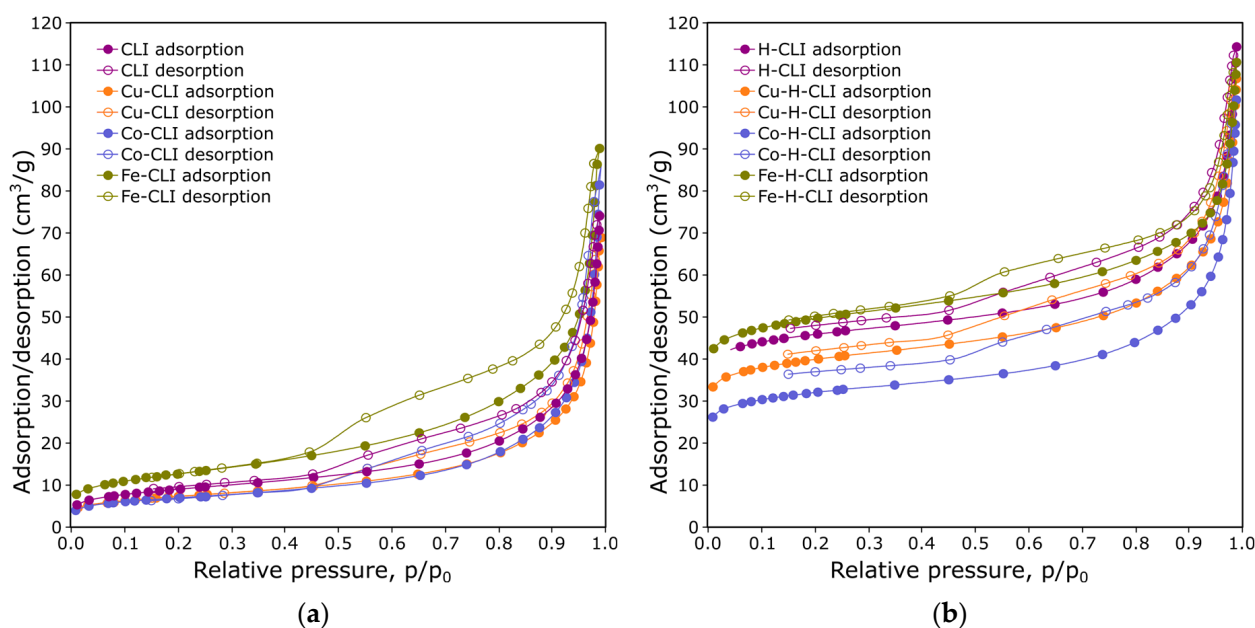


**Figure 4.** Nitrogen adsorption/desorption isotherms for clinoptilolite after ion exchange on the initial form (a) and on the hydrogen form (b) of clinoptilolite.

Table 1 presents a comprehensive summary of the BET analysis results for clinoptilolite samples. It includes clinoptilolite with deposited  $\text{Fe}^{2+}$ ,  $\text{Cu}^{2+}$ , and  $\text{Co}^{2+}$  ions (Fe-, Cu-, and Co-) both before and after ammonium exchange and calcination (CLI and H-CLI). The initial unmodified sample exhibits a surface area of  $35.44 \text{ m}^2/\text{g}$ . After introducing metals, the surface areas differ, measuring  $32.45 \text{ m}^2/\text{g}$  for Fe-CLI,  $26.05 \text{ m}^2/\text{g}$  for Cu-CLI, and  $24.83 \text{ m}^2/\text{g}$  for Co-CLI. Notably, in all analyzed samples, irrespective of the metal type, a decrease in surface area is observed. This reduction may be attributed to the potential blockage of channels or pores within the zeolite structure caused by the introduced cations.

In contrast, the catalyst matrix subjected to ammonium exchange and calcination (H-CLI) demonstrates a significant four-fold increase in surface area compared to the CLI sample. Furthermore, the zeolite catalysts based on the hydrogen form of zeolite exhibit a substantial increase in surface area compared to samples without matrix modification or ammonium exchange. This significant increase in the surface area suggests that the modification of clinoptilolite by removing alkali ions leads to partial degradation and opening of the crystalline structure, which contains a system of channels and pores. Consequently, the cations are deposited as active centers within the structure without blocking the pores, as evidenced by the results concerning the volume of micropores and mesopores.

**Table 1.** Results of nitrogen sorption for zeolite without and with ammonium exchange and modification with iron, copper, and cobalt.

Catalyst	$S_{\text{BET}}$ , ( $\text{m}^2/\text{g}$ )	$S_{\text{micro}}$ , ( $\text{m}^2/\text{g}$ )	$V_{\text{micro}}$ , ( $\text{cm}^3/\text{g}$ )	$V_{\text{meso}}$ , ( $\text{cm}^3/\text{g}$ ) *
CLI	35.44	8.62	0.004	0.11
Cu-CLI	26.05	4.41	0.002	0.10
Co-CLI	24.83	4.36	0.002	0.13
Fe-CLI	32.45	4.47	0.002	0.09
H-CLI	154.30	114.40	0.053	0.12
Cu-H-CLI	134.80	92.10	0.040	0.12
Co-H-CLI	108.50	71.40	0.030	0.12
Fe-H-CLI	168.00	119.30	0.056	0.11

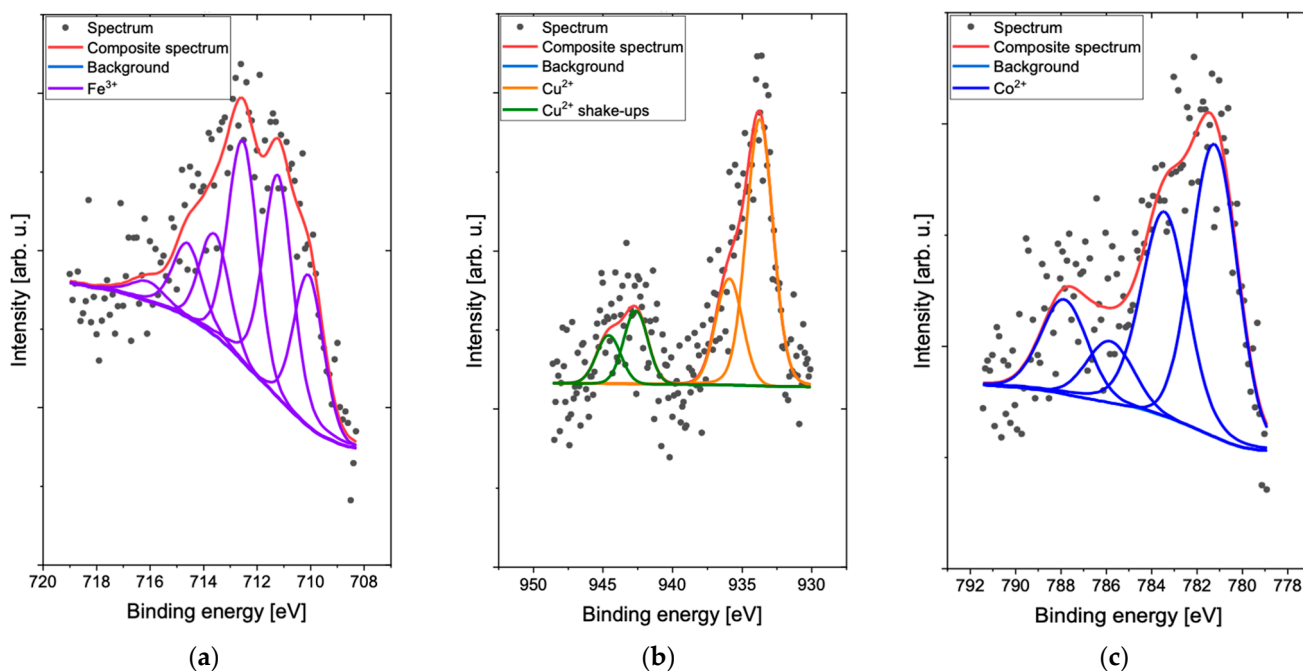
\*  $S_{\text{BET}}$ —specific surface area,  $S_{\text{micro}}$ —micropore surface area,  $V_{\text{micro}}$ —volume of micropores,  $V_{\text{meso}}$ —volume of mesopores

Surface concentrations of chemical bonds obtained from fitting XPS data for analyzed samples are listed in Table 2. The Si 2p spectra show the main  $2p_{3/2}$  line at 103.2 eV, which is responsible for the presence of Si–O bonds in silicates. In the case of the Al 2p spectra, the main  $2p_{3/2}$  line is present at 75 eV, which can be attributed to  $\text{Al}^{3+}$  ions in  $\text{Al}(\text{OH})_3$  or  $\text{Al}_2\text{O}_3$  [33]. Subsequently, the K 2p spectra were matched to one doublet structure with the main  $2p_{3/2}$  line at 294.4 eV, which may indicate the presence of  $\text{K}^+$  ions in the silicates. For the Ca 2p spectrum, the main  $2p_{3/2}$  line at 349 eV was fitted as  $\text{Ca}^{2+}$  ions in  $\text{Ca}(\text{OH})_2$  or silicates [34]. In addition, the O 1s spectrum was matched to three component lines: the first at 531.4 eV, which indicates the presence of O–Fe and/or O–Si and/or O–Al lattice oxygen. The second line observed at 532.6 eV may be due to the presence of oxygen in metal oxides (O–Fe; O–Cu; O–Co; O–Si) or organic forms (O=C), and the last line found at 533.8 eV is derived from either O–C and/or –OH bonds and/or adsorbed  $\text{H}_2\text{O}$  [33]. Also, the C 1s spectra were fitted to three components: the first observed at 285 eV as aliphatic carbon, the second at 286.9 eV as a C–O group, and the last at 289.6 eV as a group C=O and/or O–C=O and/or  $\text{CO}_3^{2-}$  groups [35].

**Table 2.** Surface composition (atomic %) determined by fitting XPS spectra for the analyzed sample.

Energy, (eV)	C			O			Al	Si	K	Ca	Fe	Cu	Co
	285.0	286.9	289.6	531.4	532.6	533.8	75.0	103.2	294.4	349.0	710.5	933.9	781.4
Groups/ Oxidation state	C–C	C–O	C=O O–C=O CO <sub>3</sub> <sup>2−</sup>	O–Me O–Si O–Al	O–Me O–Si O–Al O=C	O–C –OH H <sub>2</sub> O <sub>ads</sub>	Al <sup>3+</sup>	Si <sup>4+</sup>	K <sup>+</sup>	Ca <sup>2+</sup>	Fe <sup>3+</sup>	Cu <sup>2+</sup>	Co <sup>2+</sup>
Cu-CLI	8.7	0.9	0.5	10.2	39.0	10.8	4.5	22.5	1.1	0.7	0.5	0.7	0.0
Cu-H-CLI	7.2	1.1	0.2	9.5	38.9	12.8	4.8	24.4	0.0	0.0	0.5	0.6	0.0
Co-CLI	9.5	1.4	0.4	8.2	36.0	14.9	4.6	22.2	1.1	0.9	0.0	0.0	0.9
Co-H-CLI	9.8	1.0	0.1	9.1	37.2	13.3	4.6	24.6	0.0	0.0	0.0	0.0	0.3
Fe-CLI	8.7	1.4	0.2	11.8	33.9	14.4	4.7	22.2	0.8	0.8	1.0	0.0	0.0
Fe-H-CLI	8.6	0.9	0.2	11.0	34.7	15.3	4.7	24.1	0.0	0.0	0.6	0.0	0.0

For samples containing iron (Figure 5a,d), regardless of the matrix, an energy range of 711–715 eV was observed. The spectra in the Fe 2p<sub>3/2</sub> region were fitted with six components, with the main line at 710.5 eV. Based on the fit, the centered line corresponds to the presence of Fe<sup>3+</sup> ions. On the other hand, for the copper samples (Figure 5b,e), the observed spectra in the Cu 2p<sub>3/2</sub> region were fitted with four components, with a line centered at 933.9 eV, which may indicate the presence of either oxidation state II or III (Cu<sup>2+</sup> or Cu<sup>3+</sup>). The two additionally observed lines, present at 940–945 eV, occur only when copper is in the second oxidation state [36,37]. In the Co 2p<sub>3/2</sub> region (Figure 5c,f), spectra were collected and matched to four components, with the first line centered at 781.4 eV. This suggests the possible presence of cobalt in the second oxidation state in the form of CoO and/or Co(OH)<sub>2</sub> [38].

**Figure 5.** Cont.

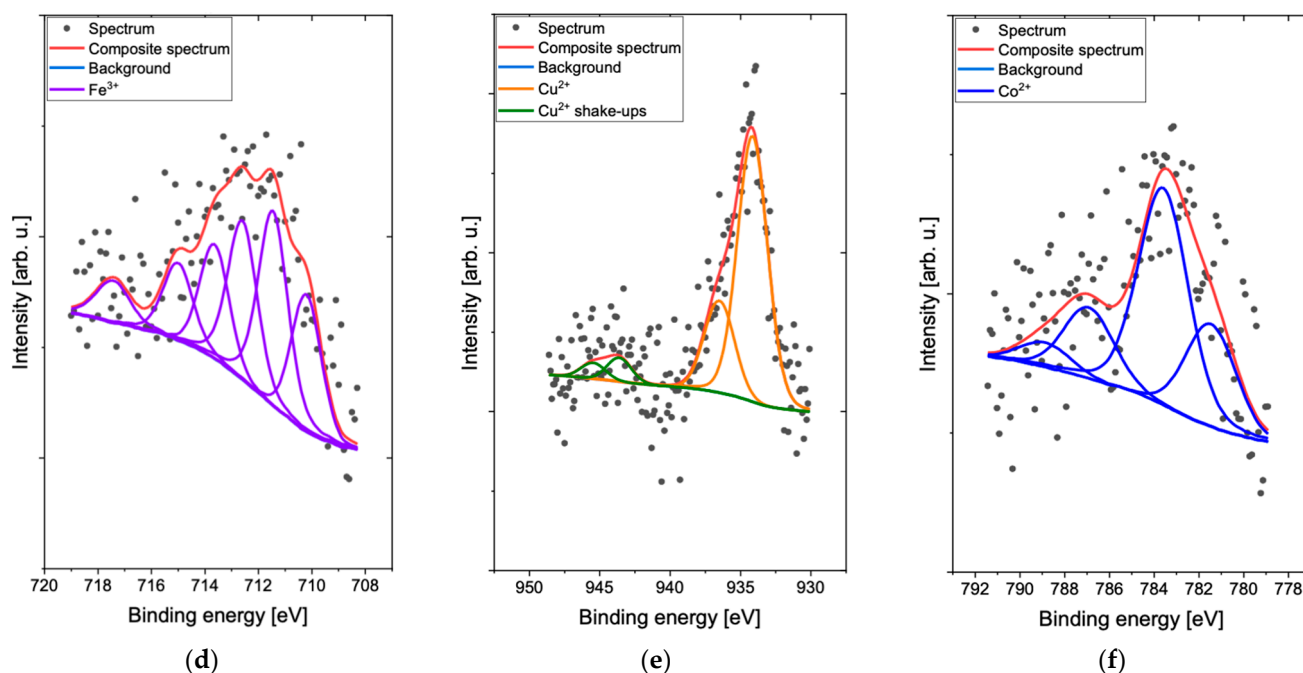


**Figure 5.** XPS spectra of Fe-CLI (a), Cu-CLI (b), Co-CLI (c), Fe-H-CLI (d), Cu-H-CLI (e), and Co-H-CLI (f).

Figure 6 illustrates the UV-Vis absorption spectra obtained from the analyzed zeolite catalysts. In the case of samples where iron was introduced onto the clinoptilolite matrix through ion exchange under ultrasonic conditions (Figure 6a), absorption bands were observed at wavelengths of 320, 360, and 385 nm, irrespective of matrix modification or ammonium exchange. According to the available literature, these bands in the range of 300–400 nm are indicative of octahedral forms of Fe<sup>3+</sup> clustered in small, oligomeric clusters of Fe<sub>2</sub>O<sub>3</sub> [39–41].

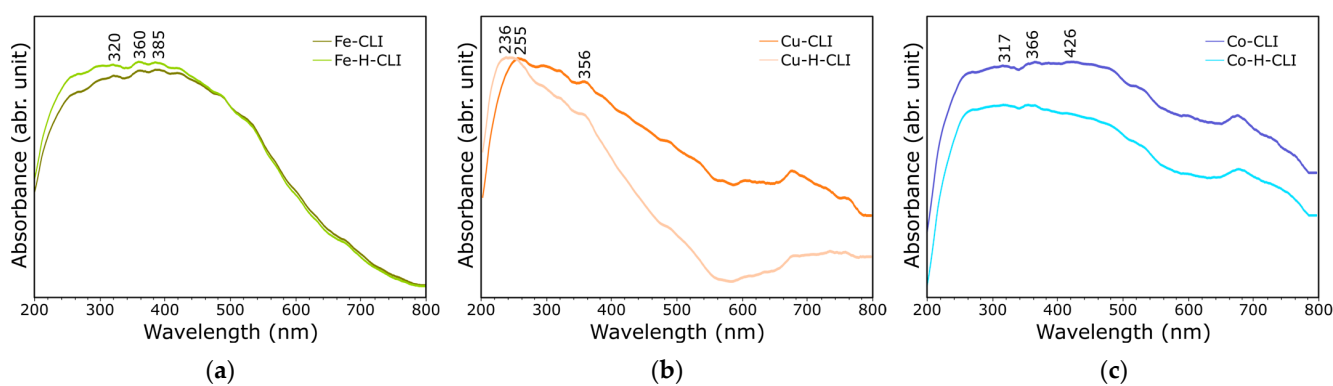


**Figure 6.** DRS-UV-Vis adsorption spectra of samples without modification (-CLI) and as hydrogen form (-H-CLI) and exchange with iron (a), copper (b), and cobalt (c).

For materials containing copper in their structure, the effect of ammonium exchange did not result in the creation of new UV-Vis absorption bands (Figure 6b). The observed wavelengths were 236 (Cu-H-CLI) and 255 nm (Cu-CLI), as well as 356 and 665 nm for both Cu-CLI and Cu-H-CLI samples. The bands at 236 nm for Cu-H-CLI and 255 nm for Cu-CLI correspond to copper in the form of isolated Cu<sup>2+</sup> ions [42]. The band at 356 nm is associated with charge transfer and originates from –O–Cu–O– complexes [43]. Furthermore, the weak band at 665 nm may be attributed to the presence of a small number of metallic forms with nanometric dimensions [43,44].

In the case of catalysts containing cobalt in their structure (Figure 6c), bands at wavelengths 317, 366 nm, 426, and 675 nm were observed for both cases. According to the literature, the bands in the wavelength range of 300–560 nm correspond to  $\text{Co}^{2+}$ - and  $\text{Co}^{3+}$ -coordinated tetrahedral ions or cobalt complexes in a symmetrical octahedral form. It is likely that the observed bands in this range indicate the presence of the  $\text{CoO}(\text{OH})$  form, which is formed during catalyst activation by oxidizing the precipitated  $\text{Co}(\text{OH})_2$  form and partially oxidizing the compensating  $\text{Co}^{2+}$  ions [45,46]. On the other hand, the band in the 400–750 nm range may suggest the presence of  $\text{Co}^{2+}$  forms in dehydrated zeolite samples [47].

Figure 7 presents the results of the  $\text{H}_2$ -TPR analysis for the clinoptilolite after ion exchange. In the case of clinoptilolite samples with iron (Figure 7a), two temperature bands were observed at 382/393 °C and 502/549 °C, regardless of the matrix used. Based on the available literature, these bands correspond to two reduction stages occurring in the temperature range of 200 to 400 °C. The first band can be attributed to the reduction of  $\text{Fe}^{3+}$  to  $\text{Fe}^{2+}$  and the reduction of  $\text{Fe}_2\text{O}_3$  to  $\text{Fe}_3\text{O}_4$ . The second extended reduction band between 400 and 700 °C can be associated with the reduction of small  $\text{Fe}_3\text{O}_4$  clusters to  $\text{FeO}_x$  [48,49].

For samples containing copper (Figure 7b), three reduction bands were observed for Cu-CLI at 200, 250, and 408 °C, while Cu-H-CLI exhibited a single peak at 408 °C. In the first case, the reduction peak at 200 °C is attributed to the reduction of dispersed CuO nanoparticles on the clinoptilolite surface, and the peaks at 250 °C indicate the reduction of isolated  $\text{Cu}^{2+}$  copper species to  $\text{Cu}^+$ . On the other hand, the reduction peak observed at 408 °C corresponds to the reduction of  $\text{Cu}^+$  to  $\text{Cu}^0$  [50,51].

For samples containing cobalt (Figure 7c), reduction peaks were observed at 370, 658, and 827 °C for Co-CLI and at 528, 646, and 837 °C for Co-H-CLI. According to the literature, the reduction peaks in the temperature range of 300–600 °C can be attributed to the reduction of cobalt particles or their low-molecular forms on the zeolite surface. Above 600 °C, the  $\text{Co}^{2+}$  form is further reduced to  $\text{Co}^+$  and  $\text{Co}^0$  [52].

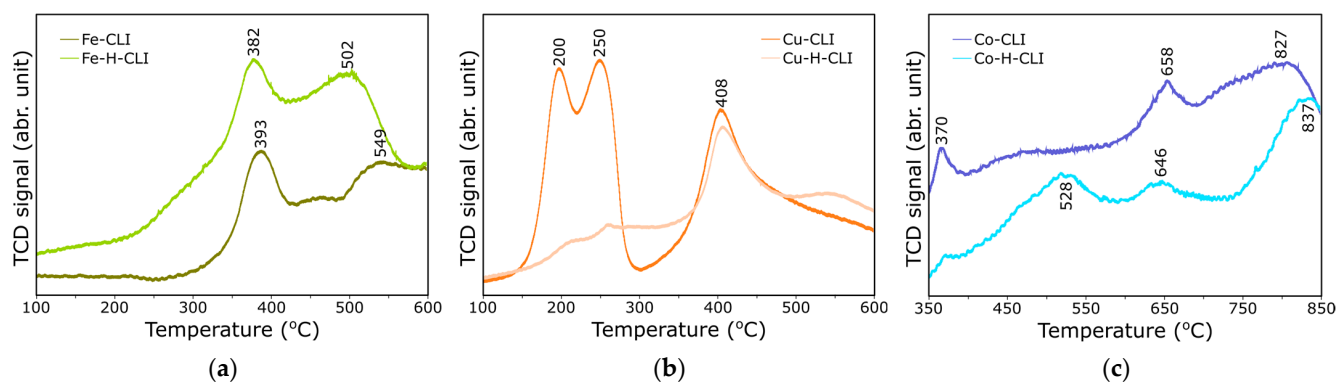


**Figure 7.**  $\text{H}_2$ -TPR profiles of samples without modification (-CLI) and as hydrogen form (-H-CLI) and exchange with iron (a), copper (b), and cobalt (c).

Table 3 presents a summary of the results obtained from the one-pot catalytic tests using glucose as the raw material. The experiments were conducted at a constant temperature of 250 °C for various durations (1, 3, 5 h) and employed catalysts with and without modified clinoptilolite as a matrix, along with ion exchange of  $\text{Fe}^{2+}$ ,  $\text{Cu}^{2+}$ , and  $\text{Co}^{2+}$  ions. Additionally, metal-free materials (CLI, H-CLI) were included in the catalytic tests.

On the basis of the collected results, it can be noticed that a large impact on the time of the GLU conversion process. In the case of short tests only for 1 h, with the exception of CLI (conversion 94.1%, selectivity to LAC 100%), GLU conversion was achieved at the level of 37.2–65.4%), where intermediate products such as fructose and 5-HMF dominate in the post-reaction mixture. Extending the process to 3 h increases the degree of GLU conversion 73.9–100% with a tendency to partially form the intermediate product—5-HMF but with the simultaneous observation of carboxylic acids, such as LA with a selectivity of

45.9% with a GLU conversion of 93.6% (Cu-CLI), FA with 15.8% selectivity at GLU 100% conversion (Fe-H-CLI), AA with 10.1% selectivity at GLU 96.6% conversion (Fe-CLI), LA with 34.9% selectivity at GLU conversion 80.5% (Cu-H-CLI), and with smaller amounts of OA and AC.

In turn, the process carried out for 5 h causes a significant increase in the degree of conversion of the raw material at the level of 87.7–100%. An intermediate product was also observed but at a level of 10.7–15.9%. In addition, after the reaction, the following compounds dominate after 5 h of the process: LAC with Fe-CLI (selectivity 53.6%, GLU conversion 95.1%), FA with Fe-CLI (selectivity 13.3%, GLU conversion 95.1%), AA with Fe-H-CLI (selectivity 11.9%, GLU conversion 96.7%), and LA with the participation of Fe-H-CLI (selectivity 40.3%, GLU conversion 96.7%).

**Table 3.** Results of the glucose conversion process at 250 °C with the participation of zeolite catalysts based on clinoptilolite.

Catalyst	Time, (h)	Conversion Degree, (%)	Conversion Products—Selectivity *, (%)							
			FRU	5-HMF	LAC	FA	AA	LA	OA	AC
CLI	1	94.1	-	-	100.0	-	-	-	-	-
	3	73.9	-	46.5	39.8	4.8	10	3.9	1.2	2.8
	5	100	-	14.4	43.6	6.2	5.0	22.5	3.2	5.3
H-CLI	1	37.2	-	93.6	6.4	-	-	-	-	-
	3	100	-	12.4	28.8	10.8	4.3	32.7	2.1	8.9
	5	100	-	12.9	24.4	10.7	7.2	35.9	3.5	5.5
Cu-CLI	1	47.7	4.0	90.3	5.7	-	-	-	-	-
	3	93.6	-	19.5	45.9	-	5.0	22.0	-	7.6
	5	100	-	15.9	40.0	-	5.1	25.7	3.9	9.3
Cu-H-CLI	1	44.2	2.3	94.2	3.5	-	-	-	-	-
	3	80.5	-	11.8	31.7	5.0	6.0	34.9	3.7	6.9
	5	100	-	10.7	36.9	-	7.4	36.4	2.6	6.0
Co-CLI	1	65.4	11.6	62.5	20.8	1.4	0.8	2.9	-	-
	3	69.9	-	32.1	31.6	7.3	4.7	15.9	2.4	5.9
	5	87.7	-	12.2	47.7	6.0	9.0	25.2	-	-
Co-H-CLI	1	49.2	9.8	65.6	18.7	2.4	-	3.6	-	-
	3	74.5	-	21.4	27.5	8.5	1.8	29.5	2.7	8.6
	5	100	-	11.1	29.6	6.6	7.9	35.6	4.4	4.9
Fe-CLI	1	62.5	5.9	35.9	14.2	5.1	-	1.5	-	-
	3	96.6	-	13.3	43.0	13.1	10.1	15.6	-	4.9
	5	95.1	-	-	53.6	13.3	6.8	26.3	-	-
Fe-H-CLI	1	55.1	9.2	61.5	23.4	3.8	-	2.1	-	-
	3	100	-	5.7	35.6	15.8	9.8	33.0	-	-
	5	96.7	-	-	29.4	11.1	11.9	40.3	-	7.3

\* FRU—fructose; 5-HMF—hydroxymethylfurfural; LAC—lactic acid; FA—formic acid; AA—acrylic acid; LA—levulinic acid; OA—oxalic acid; AC—acetic acid.

### 3. Discussion

Clinoptilolite is a promising catalyst for the conversion of glucose to organic acids. The obtained results confirmed that its structure can be successfully modified by creating a hydrogen form and ion exchange. The mere transformation of the zeolite into the

hydrogen form results in a multiple increase in the specific surface area. On the other hand, naturally occurring cations in the structure of the zeolite significantly affect the course of the analyzed reactions. The appropriate selection of the zeolite modification procedure may result in changing the properties of the catalyst in order to increase its efficiency and suitability for specific applications.

The proposed method of modifying clinoptilolite through ammonium exchange and calcination leads to a five-fold increase in the specific surface area ( $154.30 \text{ m}^2/\text{g}$ ) compared to the starting material ( $35.44 \text{ m}^2/\text{g}$ ). This enhancement opens up the possibility of using this material as a catalyst. Furthermore, the introduction of cations (iron, copper, and cobalt) during the tests was achieved via ion exchange utilizing ultrasound, which significantly reduces the time required compared to traditional modification methods. The development of modification conditions combined with ultrasound enables the rapid formation of active centers within the zeolite, as confirmed using various structural analyses, such as DRS UV-VIS, XPS, and  $\text{H}_2$ -TPR. The conducted analyses verify the presence of  $\text{Fe}^{2+}$ ,  $\text{Cu}^{2+}$ , and  $\text{Co}^{2+}$  cationic species in the zeolite structure. The structural analysis of the resulting materials demonstrates that the developed methodology does not lead to significant degradation of the crystal structure.

Based on the conducted tests, it is evident that the duration of the glucose conversion process at a constant temperature significantly affects the formation of the predominant organic acid in the post-reaction mixture. For shorter processes (1 h and 3 h), intermediate products like fructose, resulting from glucose isomerization, and 5-HMF, formed during fructose dehydration, are observed. Notably, a 1 h process using CLI as the starting sample exclusively yields lactic acid. Lactic acid is produced through a series of transformations involving glucose isomerization to fructose, followed by re-aldol transformation to dihydroxyacetone, pyruvaldehyde formation through dehydration, and subsequent hydration. Brønsted centers play a crucial role in these reactions.

Formic acid and levulinic acid are found in the post-reaction mixture as a result of glucose isomerization to fructose, followed by dehydration to 5-HMF and subsequent hydration. Both acids are influenced by the catalyst's active centers in the form of iron species, but their selectivity is additionally influenced by the catalyst matrix. Notably, the production of levulinic acid depends on the ammonium exchange process and the creation of additional Brønsted centers in the zeolite. On the other hand, the presence of iron is crucial for formic acid formation. Interestingly, acrylic acid, not previously reported in glucose catalytic conversion publications, is also observed in the post-reaction mixture. Acrylic acid is formed via the further transformation of lactic acid, specifically during its dehydration. Significantly, the highest selectivity for acrylic acid is observed after a 5 h process using previously modified zeolite through ammonium exchange and iron introduction via ion exchange in the ultrasonic field. In most cases, the presence of clinoptilolite after ammonium exchange and calcination, which provides Brønsted centers, along with iron as active centers, favors the dehydration/hydration reactions involved in glucose conversion to the aforementioned organic acids.

Based on the tests conducted at different durations (1, 3, and 5 h) and with the use of various catalytic materials, it is evident that the glucose transformation process yields a diverse array of compounds with varying selectivities, depending on the specific process conditions. Notably, the conversion of the raw material to products reaches 100% after 5 h, irrespective of the catalyst employed. However, the focus lies on identifying specific chemical compounds present in the post-reaction mixtures. One notable finding is the possibility of obtaining lactic acid after only 1 h of the process using unmodified clinoptilolite (CLI) as the catalyst. This represents a potential and novel chemical pathway for obtaining this valuable compound. On the other hand, the highest selectivity (40.3%) for levulinic acid was achieved after 5 h of the process using the hierarchized catalyst with Fe as the active center (Fe-H-CLI). Formic acid, with a selectivity of 15.8%, was obtained using the same catalytic material (Fe-H-CLI) but with a shorter process duration of 3 h. Additionally, Fe-H-CLI also led to the production of acrylic acid with a selectivity

of 11.9% after 5 h of the process. Furthermore, the identification of 5-HMF in the post-reaction mixture showed a remarkable selectivity of 94.2% when Cu-H-CLI was used as the catalyst. Additionally, oxalic acid (4.4% selectivity with Co-H-CLI) and acetic acid (9.3% selectivity with Cu-CLI) were also identified in the reaction products. These findings demonstrate the significance of process conditions and the choice of catalytic material in determining the selectivity of the glucose transformation process. The ability to selectively produce valuable chemical compounds through these reactions holds great promise for applications in various industries. The exploration of specific catalysts and the optimization of reaction conditions can further enhance the efficiency and yield of these transformations, contributing to the advancement of sustainable chemical synthesis methodologies.

It is also important to consider the presence of cobalt and copper as active centers. These metals on unmodified zeolite (Cu-CLI and Co-CLI) can also act as potential catalysts for the glucose transformation reaction. Interestingly, the selectivity of products such as lactic acid and levulinic acid significantly increases with the duration of the process when using Cu-CLI. For instance, after 1 h, the selectivity for lactic acid (LAC) is 5.7%, with a glucose conversion of 47.7%. After 3 h, the selectivity for LAC reaches 45.9%, with a glucose conversion of 93.66%, and after 5 h, the raw material is completely converted (100%) with a lactic acid selectivity of 40%. A similar trend is observed for levulinic acid with Cu-CLI, where selectivity is observed only after 3 h (22.0%) and after 5 h (25.7%), with the same glucose conversion rates observed for LAC. Using Co-CLI as a catalyst also results in a comparable situation. However, the conversion of the raw material is lower, and with increasing process time, it reaches 65.4%, 69.9%, and 87.7%, respectively. Dominant products in the post-reaction mixtures involving Co-CLI are lactic acid (with selectivities of 20.8% after 1 h, 31.6% after 2 h, and 47.7% after 5 h) and levulinic acid (with selectivities of 2.9% after 1 h, 15.9% after 3 h, and 25.2% after 5 h). On the other hand, in the case of zeolite materials subjected to the hierarchization and subsequent introduction of metals (Cu-H-CLI and Co-H-CLI), it was observed that the selectivity for lactic acid did not change significantly compared to materials without matrix hierarchization. However, as the duration of the glucose conversion process increased, the selectivity for levulinic acid showed an increase. With Cu-H-CLI, selectivity for levulinic acid was observed only from 3 h (34.9%) with a conversion of 80.5% and after 5 h (36.4%) with complete conversion (100%). A similar trend was observed when using Co-H-CLI as a catalyst, where levulinic acid selectivity was 3.6% after 1 h (with a 49.2% conversion), 29.5% after 3 h (with a 74.5% conversion), and 35.6% after 5 h (with complete conversion). Overall, the use of unmodified zeolite in combination with Cu and Co metals, along with longer process times, leads to obtaining lactic acid with higher selectivities. In contrast, the hierarchization of clinoptilolite and subsequent introduction of metals, combined with longer process times, result in obtaining levulinic acid with higher selectivity. The duration of the process and the selection of the appropriate catalytic material play a crucial role in determining the formation of specific chemical compounds.

In the presence of 5-HMF in the post-reaction mixtures, its selectivity shows a decrease with increasing process duration, regardless of the presence of a catalyst. An exception to this trend is observed in the process involving unmodified CLI, lasting 1 h, where the raw material was converted to lactic acid with a selectivity of 94.1%. Interestingly, 5-HMF is not detected after 5 h of the process when Fe-CLI and Fe-H-CLI are used as catalysts. However, in samples with H-CLI, the selectivity to 5-HMF decreases with increasing time, reaching 93.6% at 1 h, 12.4% at 3 h, and 12.9% at 5 h, respectively. For Cu-CLI and Cu-H-CLI samples, it can be observed that the selectivity to 5-HMF is lower for samples that have not undergone hierarchization before the introduction of metals. A similar trend is also evident when comparing Co-CLI and Co-H-CLI. This observation may suggest that the presence of H<sup>+</sup> ions can lead to the conversion of glucose to 5-HMF, and the presence of metals Fe, Cu, and Co act as active centers that further transform the intermediate product, 5-HMF, ultimately leading to the formation of the appropriate carboxylic acid. The specific type of active center and the duration of the process play a crucial role in determining the

subsequent transformations and selectivity of the final products. The presence of 5-HMF in the reaction mixtures, along with its varying selectivity under different catalytic conditions and process durations, highlights the complexity of the glucose transformation process. Understanding the influence of catalysts, process conditions, and active centers is vital in tailoring the synthesis of specific carboxylic acids, thereby contributing to the development of efficient and selective processes for organic acid production.

Based on the results, it is evident that the formation of specific organic acids necessitates an optimal glucose transformation time and the presence of a zeolite catalyst. These findings highlight the need for further research, particularly focusing on enhancing the catalytic activity of the material with Cu and Co metals to achieve higher selectivity towards acetic acid and oxalic acid. This avenue of investigation holds great promise in developing more efficient and selective processes for the production of these valuable organic acids.

#### 4. Materials and Methods

##### 4.1. Preparation of Zeolite Catalyst Based on Clinoptilolite

The zeolite of natural origin—clinoptilolite comes from the Carpathian deposits (Slovakia) and has been properly prepared to be used as a catalyst matrix. Zeolite was used with a 1–2 mm fraction, dried at 120 °C, and calcined for 16 h at 450 °C. The material obtained in this way was marked as CLI.

The dried and calcined clinoptilolite was subjected to ammonium exchange in order to remove alkali ions from the structure. An aqueous solution of 0.1 M  $\text{NH}_4\text{NO}_3$  was used. The appropriately weighed zeolite (1 g of zeolite per 10 ml of nitrate solution) was placed in the previously prepared ammonium nitrate(V) solution and continuously mixed as the temperature increased to 90 °C. The solid was then separated from the solution and washed several times with deionized water. The obtained ammonium form of clinoptilolite was then dried at 120 °C and calcined for 16 h at 450 °C. This sample was described as H-CLI.

Both initial clinoptilolite (CLI) and its hydrogen form (H-CLI) were used as a matrix to obtain the catalyst as a result of ion exchange. For this purpose, aqueous solutions of appropriate metal salts were prepared with molar concentrations: 0.25 M  $\text{Fe}(\text{NO}_3)_3 \cdot 9\text{H}_2\text{O}$ , 0.5 M  $\text{Cu}(\text{NO}_3)_2 \cdot 3\text{H}_2\text{O}$ , and 0.5 M  $\text{Co}(\text{NO}_3)_2 \cdot 6\text{H}_2\text{O}$ . An appropriate amount of zeolite was mixed with aqueous solutions of nitrate in a proportion of 1 g of zeolite per 100 mL of solution. The whole was transferred to an ultrasonic bath, where an ion exchange was carried out for 25 min at a temperature of 40 °C. The solid was then separated from the aqueous solutions, washed several times with deionized water, then dried at 150 °C for 2 h and calcined for 5 h at 450 °C (heating rate of 10°/min).

##### 4.2. Catalytic Tests

Catalytic tests with the participation of zeolite catalysts were carried out with the use of the one-pot technique. The appropriate raw material charge was prepared in the form of 0.125 M glucose aqueous solution and 0.1 g zeolite catalyst. The whole was placed in Teflon packing and transferred to a pressure autoclave. The GLU conversion process was carried out at a temperature of 250 °C for 1, 3, and 5 h under autogenous pressure. The post-reaction mixture was then cooled down, and samples were prepared for HPLC-RID analysis. A syringe filter with a grain diameter of 0.45  $\mu\text{m}$  was used so that the samples did not contain solid particles in the form of catalyst particles or carbon deposits. Based on the results of the analysis, the conversion of raw material, selectivity to products, product yield were determined. Based on the collected data, the conversion of glucose (GLU) was calculated as the ratio of the moles of reacted substrate to the initial moles of substrate present in the post-reaction mixture. The selectivity of individual products in the mixtures was determined as the ratio of the moles of a particular product to the sum of the moles of all products present.

### 4.3. Instrumentation

The phase composition of the materials was determined using an Empyrean X-ray diffractometer (PANalytical, Malvern, UK). Measurements were made using monochromatic Cu-K $\alpha$  radiation. The angular range was 5–90° on the 2 $\theta$  scale, and the goniometer step was 0.008°. The qualitative analysis of the phase composition was performed using the X'Pert HighScore Plus application (PANalytical, Malvern, UK) and the International Centre for Diffraction Data.

Infrared (FT-IR) spectra were measured using a Bruker VERTEX 70v vacuum spectrometer (Bruker, Billerica, MA, USA). They were collected in the region of 4000–400 cm<sup>-1</sup> after 128 scans at 4 cm<sup>-1</sup> resolution using the standard KBr pellet method. All obtained spectra were subjected to baseline correction.

Low-temperature nitrogen sorption (196 °C) was measured on a Micromeritics ASAP 2020 analyzer. The specific surface area was determined using the Brunauer–Emmett–Teller method (BET) in the pressure range  $p/p_0 = 0.05$ – $0.15$ . The size of the pores was determined using the Barrett–Joyner–Halenda method (BJH) on the basis of the volume of adsorbed nitrogen  $p/p_0 = 0.98$ .

The XPS analyses were conducted using a PHI VersaProbeII Scanning XPS system. The X-rays used had a wavelength of 1486.6 eV and were focused onto a spot size of 100  $\mu\text{m}$ , scanning an area of 400  $\mu\text{m} \times 400 \mu\text{m}$ . The photoelectron take-off angle was 45°, and the pass energy in the analyzer was set to 117.50 eV with a step size of 0.5 eV for survey scans. For high energy resolution spectra of the C 1s, O 1s, Al 2p, K 2p, Ca 2p, Cu 2p, Fe 2p, Co 2p, and Si 2p regions, the pass energy was set to 46.95 eV with a step size of 0.1 eV. To ensure a consistent sample surface potential regardless of conductivity, a dual beam charge compensation technique was employed using 7 eV Ar<sup>+</sup> ions and 1 eV electrons. All XPS spectra were referenced to the unfunctionalized, saturated carbon (C-C) C 1s peak at 285.0 eV. The operating pressure in the analytical chamber was maintained below  $3 \times 10^{-9}$  mbar. For data analysis, the PHI MultiPak software (v.9.9.3) was used to deconvolute the spectra, and the Shirley method was applied to subtract the spectrum background. Considering the applied apparatus's geometry, the information depth of the XPS analysis was estimated to be approximately 5 nm.

The temperature-programmed reduction of hydrogen (H<sub>2</sub>-TPR) was performed at a temperature from 100 to 650 °C. The sample was diluted by adding SiC to the volume of 1 mL and pretreated in a quartz reactor in a stream of helium/air mixture at 650 °C for 0.5 h. Then, the sample was cooled to 100 °C, and the TPR experiment was carried out using a 5% H<sub>2</sub>/N<sub>2</sub> mixture as a reducing gas (flow rate 30 mL/min<sup>-1</sup>) with a heating rate of 10 °C/min. H<sub>2</sub> consumption was analyzed with a TCD detector.

The optical properties of the catalysts were analyzed on the basis of the spectral dependence of the absorbance. The UV-VIS DRS spectra were recorded in diffuse reflection mode using Thermo Scientific™ Evolution 220 UV-Vis spectrophotometer (Waltham, MA, USA) in the wavelength range of 200–1000 nm. The baseline was recorded using BaSO<sub>4</sub>. The measured parameter was the total reflectance, which was converted to absorbance. Parameters such as micro-aperture, 0.05 s integration time, and a scan speed of 1200 nm/min with a step of 1 nm were determined.

Glucose conversion products were analyzed using high-performance liquid chromatography HPLC (Hewlett Packard 1050 with SUPELCOGEL™ H, 6% Crosslinked HPLC Column, 300  $\times$  7.8 mm, particle size: 9  $\mu\text{m}$ , column temperature: 35 °C, mobile phase: 0.075 M aqueous H<sub>3</sub>PO<sub>4</sub> with a flow rate of 0.3 mL/min) with a differential refraction detector (RID 1047). Automatic dosing loop: 20  $\mu\text{L}$ . The products obtained during the process were identified on the basis of standard substances, based on a five-point calibration curve.

## 5. Conclusions

We prepared a series of catalysts based on natural clinoptilolite as hydrogen form, after acid treatment and ion exchange. Fe, Cu, and Co were introduced onto the zeolite

matrix using ultrasound. The results of X-ray diffraction analysis show that the proposed modification conditions did not lead to the degradation of the clinoptilolite crystal structure. Additionally, BET analysis confirmed a significant increase in the specific surface area of the materials compared to the original zeolite ( $35.55 \text{ m}^2/\text{g}$ ). The highest increase in surface area was observed for the sample after ammonium exchange and subsequent hierarchization (H-CLI) with  $154.3 \text{ m}^2/\text{g}$ , and for Fe-H-CLI with  $168 \text{ m}^2/\text{g}$ .

Subsequent DRS UV-VIS,  $\text{H}_2$ -TPR, and XPS analyses allowed the determination of the presence and metallic forms of the active centers. Regardless of the method of modification of the zeolite matrix, the metals were introduced in the form of  $\text{Fe}^{3+}$ ,  $\text{Cu}^{2+}$ , and  $\text{Co}^{2+}$ . The catalysts were then used in the glucose conversion process, and their activity was evaluated based on the results obtained from HPLC-RID. It was found that the duration of the glucose conversion process at the same temperature significantly influenced the dominant organic acid obtained in the post-reaction mixture. Short processes of 1 h and 3 h resulted in the observation of intermediate products—fructose, which is the result of glucose isomerization, and 5-HMF, formed during fructose dehydration. Interestingly, the process carried out for 1 h using CLI as the starting sample led to the production of only lactic acid. Lactic acid is formed as a result of a series of transformations involving glucose isomerization to fructose, followed by re-aldol transformation to dihydroxyacetone, and then pyruvaldehyde as a result of dehydration, and finally, during its hydration. Brønsted centers played an important role in this transformation.

Formic acid and levulinic acid were also formed in the post-reaction mixture as a result of glucose isomerization to fructose, followed by further dehydration to 5-HMF and subsequent hydration. Both acids were formed with the participation of the catalyst with iron, but their selectivity was additionally influenced by the catalyst matrix. The production of levulinic acid was also promoted on the hydrogen form of zeolite. On the other hand, for formic acid, only the presence of iron was important.

Surprisingly, acrylic acid was also observed in the post-reaction mixture, which was not previously reported in publications on the catalytic conversion of glucose. This acid is formed as a further transformation of lactic acid, precisely during its dehydration. Importantly, the highest selectivity was observed after 5 h of the process with the participation of previously modified zeolite by ammonium exchange and the introduction of iron by ion exchange in the ultrasonic field.

In most cases, organic acids with satisfactory selectivity were formed due to the presence of clinoptilolite after ammonium exchange, which obtains Brønsted centers and iron as active centers, favoring the dehydration/hydration reaction of glucose conversion to the above organic acids. In conclusion, each catalyst had a specific role and led to specific chemical compounds. For example, the Co-CLI catalyst produced fructose (FRU) with the highest selectivity of 11.6% and glucose (GLU) conversion of 65.4% after 1 h of the process. The Cu-H-CLI catalyst resulted in 5-HMF after 1 h with a selectivity of 94.2% (GLU conversion 44.2%). The CLI catalyst was responsible for obtaining lactic acid (LAC) with 100% selectivity after 1 h of the process. The Fe-H-CLI catalyst led to formic acid (FA) with a selectivity of 15.8% and complete GLU conversion after 3 h. After 5 h of the process, the Fe-H-CLI catalyst produced levulinic acid (LA) with a selectivity of 40.3% and acrylic acid (AA) with a selectivity of 11.9% at 96.7% conversion of the raw material. In post-reaction mixtures after 4 h of the process with Co-H-CLI, oxalic acid (OA) was identified with 4.4% selectivity. Acetic acid (AC) with the highest selectivity of 9.3% and 100% GLU conversion was observed after 5 h of the process with Cu-CLI.

**Author Contributions:** Conceptualization, N.S. and M.K.; methodology, N.S. and M.K.; software, N.S. and M.K.; validation, N.S. and M.K.; formal analysis, N.S. and M.K.; investigation, N.S., I.L. and M.K.; resources, N.S. and M.K.; data curation, N.S. and M.K.; writing—original draft preparation, N.S.; writing—review and editing, N.S. and M.K.; visualization, N.S. and M.K.; supervision, N.S.; project administration, N.S.; funding acquisition, N.S. All authors have read and agreed to the published version of the manuscript.

**Funding:** This work was financially supported by the National Science Centre, Poland, under grant no. UMO-2021/41/N/ST5/00084.

**Data Availability Statement:** The data presented in this study are available upon request from the corresponding author.

**Conflicts of Interest:** The authors declare no conflict of interest.

## References

1. Steinbach, D.; Klier, A.; Kruse, A.; Sauer, J.; Wild, S.; Zanker, M. Isomerization of glucose to fructose in hydrolysates from lignocellulosic biomass using hydrotalcite. *Processes* **2020**, *8*, 644. [[CrossRef](#)]
2. Huang, H.; Meng, X.-G.; Yu, W.-W.; Chen, L.-Y.; Wu, Y.-Y. High selective isomerization of glucose to fructose catalyzed by amidoximed polyacrylonitrile. *ACS Omega* **2021**, *6*, 19860–19866. [[CrossRef](#)]
3. Zhang, S.; Sheng, K.; Chen, X.; Zhang, X.; Mosier, N.S. Conversion of glucose to 5-hydroxymethyl furfural in water-acetonitrile-dimethyl sulfoxide solvent with aluminum on activated carbon and maleic acid. *Ind. Crops Prod.* **2021**, *174*, 114220. [[CrossRef](#)]
4. Jeong, G.-T.; Kim, S.-K. Statistical optimization of levulinic acid and formic acid production from lipid-extracted residue of *Chlorella vulgaris*. *J. Environ. Chem. Eng.* **2021**, *9*, 105142. [[CrossRef](#)]
5. Xia, M.; Dong, W.; Gu, M.; Chang, C.; Shen, Z.; Zhang, Y. Synergetic effects of bimetals in modified beta zeolite for lactic acid synthesis from biomass-derived carbohydrates. *RSC Adv.* **2018**, *8*, 8965–8975. [[CrossRef](#)] [[PubMed](#)]
6. Jin, F.; Zhou, Z.; Enomoto, H.; Moriya, T.; Higashijima, H. Conversion mechanism of cellulosic biomass to lactic acid in subcritical water and acid–base catalytic effect of subcritical water. *Chem. Lett.* **2004**, *33*, 126–127. [[CrossRef](#)]
7. Yang, G.-Y.; Ke, Y.-H.; Ren, H.-F.; Liu, C.-L.; Yang, R.-Z.; Dong, W.-S. The conversion of glycerol to lactic acid catalyzed by ZrO<sub>2</sub>-supported CuO catalysts. *Chem. Eng. J.* **2016**, *283*, 759–767. [[CrossRef](#)]
8. Ramírez-López, C.A.; Ochoa-Gómez, J.R.; Fernández-Santos, M.; Gómez-Jiménez-Aberasturi, O.; Alonso-Vicario, A.; Torrecilla-Soria, J. Synthesis of lactic acid by alkaline hydrothermal conversion of glycerol at high glycerol concentration. *Ind. Eng. Chem. Res.* **2010**, *49*, 6270–6278. [[CrossRef](#)]
9. Xu, S.; He, T.; Li, J.; Huang, Z.; Hu, C. Enantioselective synthesis of D-lactic acid via chemocatalysis using MgO: Experimental and molecular-based rationalization of the triose's reactivity and preliminary insights with raw biomass. *Appl. Catal. B* **2021**, *292*, 120145. [[CrossRef](#)]
10. Santos, K.M.A.; Albuquerque, E.M.; Innocenti, G.; Borges, L.E.P.; Sievers, C.; Fraga, M.A. The role of Brønsted and water-tolerant Lewis acid sites in the cascade aqueous-phase reaction of triose to lactic acid. *ChemCatChem* **2019**, *11*, 3054–3063. [[CrossRef](#)]
11. Hossain, M.A.; Mills, K.N.; Molley, A.M.; Rahaman, M.S.; Tulaphol, S.; Lalvani, S.B.; Dong, J.; Sunkara, M.K.; Sathitsuksanoh, N. Catalytic isomerization of dihydroxyacetone to lactic acid by heat treated zeolites. *Appl. Catal. A* **2021**, *611*, 117979. [[CrossRef](#)]
12. Li, S.; Deng, W.; Li, Y.; Zhang, Q.; Wang, Y. Catalytic conversion of cellulose-based biomass and glycerol to lactic acid. *J. Energy Chem.* **2019**, *32*, 138–151. [[CrossRef](#)]
13. Huo, Z.; Fang, Y.; Yao, G.; Zeng, X.; Ren, D.; Jin, F. Improved two-step hydrothermal process for acetic acid production from carbohydrate biomass. *J. Energy Chem.* **2015**, *24*, 207–212. [[CrossRef](#)]
14. Wang, Y.; Jin, F.; Sasaki, M.; Wang, F.; Jing, Z.; Goto, M. Selective conversion of glucose into lactic acid and acetic acid with copper oxide under hydrothermal conditions. *AIChE J.* **2012**, *59*, 2096–2104. [[CrossRef](#)]
15. Sobuś, N.; Michorczyk, B.; Piotrowski, M.; Kuterasiński, Ł.; Chlebda, D.K.; Łojewska, J.; Jędrzejczyk, R.J.; Jodłowski, P.; Kuśtrowski, P.; Czekaj, I. Design of Co, Cu and Fe–BEA zeolite catalysts for selective conversion of lactic acid into acrylic acid. *Catal. Lett.* **2019**, *149*, 3349–3360. [[CrossRef](#)]
16. Eminov, S.; Brandt, A.; Wilton-Ely, J.D.E.T.; Hallett, J.P. The highly selective and near-quantitative conversion of glucose to 5-hydroxymethylfurfural using ionic liquids. *PLoS ONE* **2016**, *11*, e0163835. [[CrossRef](#)] [[PubMed](#)]
17. Shiwei, W.; Qibao, W. Selective conversion of glucose into lactic acid with immobilized ytterbium triflate. *Reac. Kinet. Mech. Cat.* **2018**, *125*, 923–936. [[CrossRef](#)]
18. Sobuś, N.; Król, M.; Piotrowski, M.; Michorczyk, B.; Czekaj, I.; Kornaus, K.; Zając-Trenczek, A.; Komarek, S. Conversion of dihydroxyacetone to carboxylic acids on pretreated clinoptilolite modified with iron, copper, and cobalt. *Catal. Commun.* **2022**, *171*, 106509. [[CrossRef](#)]
19. Ramesh, A.; Rajesh, D.; Shanthi, K.; Bhargav, P.B.; Nguyen-Le, M.-T. Catalytic conversion of glucose to 5-hydroxymethylfurfural productions over sulphated Ti–Al<sub>2</sub>O<sub>3</sub> catalysts. *Biomass Bioenergy* **2021**, *154*, 106261. [[CrossRef](#)]
20. Li, K.; Du, M.; Ji, P. Multifunctional tin-based heterogeneous catalyst for catalytic conversion of glucose to 5-hydroxymethylfurfural. *ACS Sustain. Chem. Eng.* **2018**, *6*, 5636–5644. [[CrossRef](#)]
21. Atanda, L.; Mukundan, S.; Shrotri, A.; Ma, Q.; Beltramini, J. Catalytic Conversion of Glucose to 5-Hydroxymethyl-furfural with a Phosphated TiO<sub>2</sub> Catalyst. *ChemCatChem* **2015**, *7*, 781–790. [[CrossRef](#)]
22. Kumar, K.; Kumar, M.; Upadhyayula, S. catalytic conversion of glucose into levulinic acid using 2-phenyl-2-imidazoline based ionic liquid catalyst. *Molecules* **2021**, *26*, 348. [[CrossRef](#)] [[PubMed](#)]
23. Girisuta, B.; Janssen, L.P.B.M.; Heeres, H.J. Green Chemicals. *Chem. Eng. Res. Des.* **2006**, *84*, 339–349. [[CrossRef](#)]
24. Weingarten, R.; Kim, Y.T.; Tompsett, G.A.; Fernández, A.; Han, K.S.; Hagaman, E.W.; Conner, W.C.; Dumesic, J.A.; Huber, G.W. Conversion of glucose into levulinic acid with solid metal(IV) phosphate catalysts. *J. Catal.* **2013**, *304*, 123–134. [[CrossRef](#)]

25. Shen, Z.; Kong, L.; Zhang, W.; Gu, M.; Xia, M.; Zhou, X.; Zhang, Y. Surface amino-functionalization of Sn-Beta zeolite catalyst for lactic acid production from glucose. *RSC Adv.* **2019**, *9*, 18989–18995. [[CrossRef](#)]
26. Deng, W.; Wang, P.; Wang, B.; Wang, Y.; Yan, L.; Li, Y.; Zhang, Q.; Cao, Z.; Wang, Y. Transformation of cellulose and related carbohydrates into lactic acid with bifunctional Al(III)–Sn(II) catalysts. *Green Chem.* **2018**, *20*, 735–744. [[CrossRef](#)]
27. Sun, Y.; Shi, L.; Wang, H.; Miao, G.; Kong, L.Z.; Li, S.; Sun, Y. Efficient production of lactic acid from sugars over Sn-Beta zeolite in water: Catalytic performance and mechanistic insights. *Sustain. Energy Fuels* **2019**, *3*, 1163–1171. [[CrossRef](#)]
28. Nikolov, A.; Nugteren, H.; Rostovsky, I. Optimization of geopolymers based on natural zeolite clinoptilolite by calcination and use of aluminate activators. *Constr. Build. Mater.* **2020**, *243*, 118257. [[CrossRef](#)]
29. Mohammadzadeh Kakhki, R.; Tayebbe, R.; Mohammadpour, M.; Ahsani, F. Fast and highly efficient removal of anionic organic dyes with a new Cu modified nanoclinoptilolite. *J. Incl. Phenom. Macrocycl. Chem.* **2018**, *91*, 133–139. [[CrossRef](#)]
30. Moradi, M.; Hosseini Sabzevari, M.; Marahel, F.; Shameli, A. Removal of reactive green KE-4BD and Congo red dyes in textile effluent by natural clinoptilolite particles on a biosorbent as a cheap and efficient adsorbent: Experimental design and optimisation. *Int. J. Environ. Anal. Chem.* **2021**, 1–19. [[CrossRef](#)]
31. Pandey, S.; Fosso-Kankeu, E.; Spiro, M.J.; Waanders, F.; Kumar, N.; Ray, S.S.; Kim, J.; Kang, M. Equilibrium, kinetic, and thermodynamic studies of lead ion adsorption from mine wastewater onto MoS<sub>2</sub>-clinoptilolite composite. *Mater. Today Chem.* **2020**, *18*, 100376. [[CrossRef](#)]
32. Muttakin, M.; Mitra, S.; Thu, K.; Ito, K.; Saha, B.B. Theoretical framework to evaluate minimum desorption temperature for IUPAC classified adsorption isotherms. *Int. J. Heat Mass Transf.* **2018**, *122*, 795–805. [[CrossRef](#)]
33. Medykowska, M.; Wiśniewska, M.; Szewczuk-Karpisz, K.; Panek, R. Interaction mechanism of heavy metal ions with the nanostructured zeolites surface—Adsorption, electrokinetic and XPS studies. *J. Mol. Liquid.* **2022**, *357*, 119144. [[CrossRef](#)]
34. Ruiz-Serrano, D.; Flores-Acosta, M.; Conde-Barajas, E.; Ramírez-Rosales, D.; Yáñez-Limón, J.M.; Ramírez-Bon, R. Study by XPS of different conditioning processes to improve the cation exchange in clinoptilolite. *J. Mol. Struct.* **2010**, *980*, 149–155. [[CrossRef](#)]
35. Rajan, M.S.; John, A.; Yoon, M. Zeolite Y-supported carbon-doped TiO<sub>2</sub> nanocomposites: Efficient solar photocatalysts for the purification of medicinal wastewater. *Environ. Sci. Pollut. Res.* **2023**, *30*, 60638–60653. [[CrossRef](#)]
36. Zhu, X.; Li, H.; Shang, X. Fe-Cu binary oxide loaded zeolite as heterogeneous Fenton catalyst for degradation of carbamazepine at near-neutral pH. *Environ. Sci. Pollut. Res.* **2022**, *29*, 73181–73190. [[CrossRef](#)] [[PubMed](#)]
37. Zhang, M.; Wang, X. Preparation of a gangue-based X-type zeolite molecular sieve as a multiphase fenton catalyst and its catalytic performance. *ACS Omega* **2021**, *6*, 18414–18425. [[CrossRef](#)] [[PubMed](#)]
38. Grzybek, G.; Greluk, M.; Patulski, P.; Stelmachowski, P.; Tarach, K.; Słowik, G.; Rotko, M.; Valencia, S.; Rey, F.; Góra-Marek, K. Adjustment of the ZSM-5 zeolite support towards the efficient hydrogen production by ethanol steam reforming on cobalt catalysts. *Chem. Eng. J.* **2023**, *467*, 143239. [[CrossRef](#)]
39. Shahbazi, A.; Gonzalez-Olmos, R.; Kopinke, F.-D.; Zarabadi-Poor, P.; Georgi, A. Natural and synthetic zeolites in adsorption/oxidation processes to remove surfactant molecules from water. *Sep. Purif. Technol.* **2014**, *127*, 1–9. [[CrossRef](#)]
40. Saramok, M.; Inger, M.; Antoniak-Jurak, K.; Szymaszek-Wawryca, A.; Samojedon, B.; Motak, M. Physicochemical features and NH<sub>3</sub>-SCR catalytic performance of natural zeolite modified with iron—The effect of Fe loading. *Catalysts* **2022**, *12*, 731. [[CrossRef](#)]
41. Szymaszek-Wawryca, A.; Díaz, U.; Samojedon, B.; Motak, M. Catalytic performance of one-pot synthesized Fe-MWW layered zeolites (MCM-22, MCM-36, and ITQ-2) in selective catalytic reduction of nitrogen oxides with ammonia. *Molecules* **2022**, *27*, 2983. [[CrossRef](#)] [[PubMed](#)]
42. Chen, J.; Huang, W.; Bao, S.; Zhang, W.; Liang, T.; Zheng, S.Y.L.; Guo, L.W.X. A review on the characterization of metal active sites over Cu-based and Fe-based zeolites for NH<sub>3</sub>-SCR. *RSC Adv.* **2022**, *12*, 27746–27765. [[CrossRef](#)]
43. Pestryakov, A.N.; Petranovskii, V.P.; Kryazhov, A.; Ozhereliev, O.; Pfänder, N.; Knop-Gericke, A. Study of copper nanoparticles formation on supports of different nature by UV-Vis diffuse reflectance spectroscopy. *Chem. Phys. Lett.* **2004**, *385*, 173–176. [[CrossRef](#)]
44. Rodríguez-Iznaga, I.; Petranovskii, V.; Espinosa, M.Á.H.; Barraza, F.C.; Pestryakov, A. Effect of the zeolitic matrix on the reduction process of Cu<sup>2+</sup> cations in clinoptilolite, mordenite and erionite. *Adv. Mat. Res.* **2014**, *880*, 48–52.
45. Rokicińska, A.; Drozdek, M.; Bogdan, E.; Węgrzynowicz, A.; Michorczyk, P.; Kuśtrowski, P. Combustion of toluene over cobalt-modified MFI zeolite dispersed on monolith produced using 3D printing technique. *Catal. Today* **2020**, *375*, 369–376. [[CrossRef](#)]
46. Bellmann, A.; Rautenberg, C.; Bentrup, U.; Brückner, A. Determining the location of Co<sup>2+</sup> in zeolites by UV-Vis diffuse reflection spectroscopy: A critical view. *Catalysts* **2020**, *10*, 123. [[CrossRef](#)]
47. Martins, L.; Peguin, R.P.S.; Wallau, M.; Urquieta-González, E.A. Selective catalytic reduction of NO to N<sub>2</sub> with copper and cobalt exchanged ZSM-5 zeolites: The effect of calcium addition. *J. Braz. Chem. Soc.* **2005**, *16*, 589–596. [[CrossRef](#)]
48. Zeng, J.; Chen, S.; Fan, Z.; Wang, C.; Chang, H.; Li, J. Simultaneous selective catalytic reduction of NO and N<sub>2</sub>O by NH<sub>3</sub> over Fe-zeolite catalysts. *Ind. Eng. Chem. Res.* **2020**, *59*, 19500–19509. [[CrossRef](#)]
49. Putluru, S.S.R.; Schill, L.; Jensen, A.D.; Fehrmann, R.S.N. Selective catalytic reduction of NO<sub>x</sub> with NH<sub>3</sub> on Cu-, Fe-, and Mn-zeolites prepared by impregnation: Comparison of activity and hydrothermal stability. *J. Chem.* **2018**, *2018*, 8614747. [[CrossRef](#)]
50. Lai, S.; Meng, D.; Zhan, W.; Guo, Y.; Guo, Y.; Zhang, Z.; Lu, G. The promotional role of Ce in Cu/ZSM-5 and in situ surface reaction for selective catalytic reduction of NO<sub>x</sub> with NH<sub>3</sub>. *RSC Adv.* **2015**, *5*, 90235–90244. [[CrossRef](#)]

51. Yang, X.; Wang, X.; Qiao, X.; Jin, Y.; Fan, B. Effect of hydrothermal aging treatment on decomposition of NO by Cu-ZSM-5 and modified mechanism of doping Ce against this influence. *Materials* **2020**, *13*, 888. [[CrossRef](#)] [[PubMed](#)]
52. Li, S.; Zhang, C.; Li, J.; Li, Y.; Wang, H.; Li, C.; Song, Y. Direct catalytic decomposition of N<sub>2</sub>O over Co(x)/RPSA catalysts. *Res. Chem. Intermed.* **2019**, *45*, 3601–3616. [[CrossRef](#)]

**Disclaimer/Publisher's Note:** The statements, opinions and data contained in all publications are solely those of the individual author(s) and contributor(s) and not of MDPI and/or the editor(s). MDPI and/or the editor(s) disclaim responsibility for any injury to people or property resulting from any ideas, methods, instructions or products referred to in the content.